REGULAR ARTICLE

blood advances

A refined cell-of-origin classifier with targeted NGS and artificial intelligence shows robust predictive value in DLBCL

Zijun Y. Xu-Monette,[1,*] Hongwei Zhang,[2,*] Feng Zhu,[1,*] Alexandar Tzankov,[3] Govind Bhagat,[4] Carlo Visco,[5] Karen Dybkaer,[6] April Chiu,[7] Wayne Tam,[8] Youli Zu,[9] Eric D. Hsi,[10] Hua You,[11] Jooryung Huh,[12] Maurilio Ponzoni,[13] Andrés J. M. Ferreri,[13] Michael B. Møller,[14] Benjamin M. Parsons,[15] J. Han van Krieken,[16] Miguel A. Piris,[17] Jane N. Winter,[18] Fredrick B. Hagemeister,[19] Babak Shahbaba,[20] Ivan De Dios,[21] Hong Zhang,[22] Yong Li,[23] Bing Xu,[24] Maher Albitar,[21] and Ken H. Young[1,25]

[1]Division of Hematopathology and Department of Pathology, Duke University Medical Center, Durham, NC; [2]Department of Hematology, Shanxi Cancer Hospital, Taiyuan, China; [3]Institute of Pathology, University Hospital Basel, Basel, Switzerland; [4]Department of Pathology, Columbia University Medical Center and New York Presbyterian Hospital, New York, NY; [5]Department of Hematology, University of Verona, Verona, Italy; [6]Department of Hematology, Aalborg University Hospital, Aalborg, Denmark; [7]Department of Pathology, Mayo Clinic, Rochester, MN; [8]Department of Pathology, Weill Medical College of Cornell University, New York, NY; [9]Department of Pathology, Houston Methodist Hospital, Houston, TX; [10]Department of Pathology, Cleveland Clinic, Cleveland, OH; [11]Department of Hematology, Affiliated Cancer Hospital & Institute of Guangzhou Medical University, Guangzhou, China; [12]Department of Pathology, Asan Medical Center, Ulsan University College of Medicine, Seoul, Korea; [13]Department of Hematology and Pathology, San Raffaele H. Scientific Institute, Milan, Italy; [14]Department of Pathology, Odense University Hospital, Odense, Denmark; [15]Department of Hematology, Gundersen Lutheran Health System, La Crosse, WI; [16]Department of Pathology, Radboud University Nijmegen Medical Centre, Nijmegen, The Netherlands; [17]Department of Pathology, Fundación Jiménez Díaz, Centro de Investigación Biomédica en Red de Cáncer (CIBERONC), Madrid, Spain; [18]Department of Hematology, Feinberg School of Medicine, Northwestern University, Chicago, IL; [19]Department of Lymphoma and Myeloma, The University of Texas MD Anderson Cancer Center, Houston, TX; [20]Department of Biostatistics, Donald Bren School of Information and Computer Sciences, University of California, Irvine, CA; [21]Genomic Testing Cooperative, Irvine, CA; [22]Department of Computer Science, Georgia Southern University, Savannah, GA; [23]Department of Medicine, Baylor College of Medicine, Houston, TX; [24]Department of Hematology, The First Affiliated Hospital of Xiamen University, Xiamen, Fujian, China; and [25]Hematologic Malignancy Program, Duke Cancer Institute, Durham, NC

Key Points

- A DLBCL cell-of-origin classifier integrating both genetic and gene expression signatures shows robust predictive values in DLBCL cohorts.
- Targeted NGS and AI enable potential application of fast and reliable DLBCL classification assays in clinical practice.

Diffuse large B-cell lymphoma (DLBCL) is a heterogeneous entity of B-cell lymphoma. Cell-of-origin (COO) classification of DLBCL is required in routine practice by the World Health Organization classification for biological and therapeutic insights. Genetic subtypes uncovered recently are based on distinct genetic alterations in DLBCL, which are different from the COO subtypes defined by gene expression signatures of normal B cells retained in DLBCL. We hypothesize that classifiers incorporating both genome-wide gene-expression and pathogenetic variables can improve the therapeutic significance of DLBCL classification. To develop such refined classifiers, we performed targeted RNA sequencing (RNA-Seq) with a commercially available next-generation sequencing (NGS) platform in a large cohort of 418 DLBCLs. Genetic and transcriptional data obtained by RNA-Seq in a single run were explored by state-of-the-art artificial intelligence (AI) to develop a NGS-COO classifier for COO assignment and NGS survival models for clinical outcome prediction. The NGS-COO model built through applying AI in the training set was robust, showing high concordance with COO classification by either Affymetrix GeneChip microarray or the NanoString Lymph2Cx assay in 2 validation sets. Although the NGS-COO model was not trained for clinical outcome, the activated B-cell–like compared with the germinal-center B-cell–like subtype had significantly poorer survival. The NGS survival models stratified 30% high-risk patients in the validation set with poor survival as in the training set. These results demonstrate that targeted RNA-Seq coupled with AI deep learning techniques provides reproducible, efficient, and affordable assays for clinical application. The clinical grade assays and NGS models integrating both genetic and transcriptional factors developed in this study may eventually support precision medicine in DLBCL.

Submitted 30 March 2020; accepted 13 June 2020; published online 28 July 2020.
DOI 10.1182/bloodadvances.2020001949.

*Z.Y.X.-M., Hongwei Zhang, and F.Z. contributed equally to this study.

Data are in the supplemental data file with 2 worksheets available with the article.

The full-text version of this article contains a data supplement.

Introduction

Diffuse large B-cell lymphoma (DLBCL) is the most common B-cell lymphoma and is clinically heterogeneous. Gene expression profiling (GEP) classified DLBCL into 2 major molecular subtypes according to their cell of origin (COO): germinal-center B-cell–like (GCB) and activated B-cell–like (ABC) DLBCL.[1] ABC-COO is associated with poorer clinical outcomes in DLBCL irrespective of treatment: CHOP (cyclophosphamide, doxorubicin, vincristine, and prednisone), rituximab (R)-CHOP,[1-3] obinutuzumab (G)-CHOP,[4] or classical salvage chemotherapy R-DHAP (rituximab, dexamethasone, high-dose cytarabine, and cisplatin) followed by intensive therapy plus autologous stem cell transplantation.[5] However, several novel agents, including lenalidomide,[6-8] ibrutinib,[8,9] and bortezomib alone[10] or in combination with durvalumab (anti–PD-L1),[11] showed selective or better clinical efficacy in ABC- vs GCB-DLBCL. The prognostic and therapeutic differences between ABC- and GCB-DLBCL have a molecular basis, such as higher frequencies of mutations in *CD79*, *MYD88*, *CARD11*, *PRDM1*, and *TNFAIP3*,[12] chronic active B-cell receptor signaling,[13] and more frequent MYC/BCL2 double expression in the absence of genetic *MYC*/*BCL2* double hit[14] in ABC-DLBCL. In addition, the subcellular distribution and mechanism of action of doxorubicin in ABC-DLBCL are different from those in GCB-DLBCL.[15] To guide clinical therapeutics, distinction of the GCB vs ABC/non-GC subtype has become the standard practice according to the 2016 revision of the World Health Organization classification of lymphoid neoplasms.[16]

Significant efforts have been put into establishing clinically applicable assays and accurate classification of DLBCL, and methodology to determine COO has been evolving in the last 2 decades. The original Lymphochip spotted cDNA microarray and the gold standard classification algorithm are robust in COO classification but impracticable for routine clinical practice.[1-3] Researchers thus developed algorithms to distinguish GC from non-GC subtypes based on protein expression of 3 to 5 biomarkers in formalin-fixed, paraffin-embedded (FFPE) tissue samples readily assessed by immunohistochemistry (IHC) in the clinic.[17-24] However, the accuracy of these IHC algorithms and the prognostic significance of COO subtypes determined by IHC algorithms[5,25] are not consistent.[23,26-28] To enable GEP by DNA microarrays to classify DLBCL using clinical FFPE tissues that yield highly fragmented RNA samples, new RNA amplification and labeling techniques and classification models were developed, including a 100-gene classifier for Affymetrix GeneChip (Affymetrix, Inc) data[29] and a 20-gene DLBCL Automatic classifier for Illumina WG-DASL platform (Illumina United Kingdom) data[30] developed from a previous platform-independent 27-gene DLBCL subgroup predictor[31] that showed reproducibility and prognostic value.

To simplify the GEP process for FFPE samples, a multiplexed quantitative nuclease protection assay (qNPA) was developed that directly hybridizes mRNA in situ using 50-mer probes for genes of interest, followed by probe capture and quantitative imaging, thereby reliably detecting mRNA levels in FFPE samples without RNA exaction and amplification.[32-34] The qNPA platform (HTG Molecular Diagnostics, Inc.) can accurately classify DLBCL using a 14-gene signature.[35] The current HTG EdgeSeq DLBCL COO assay has been applied in a clinic trial.[36] However, the most successful simplified variation of microarray for rapid COO determination is the NanoString nCounter System (NanoString Technologies), which elegantly detects target mRNA of interest in extracted nonamplified RNA samples using a capture probe and a color-coded reporter probe, followed by purification, immobilization, and digital readout.[37] Several different small gene panel-based DLBCL-COO assays, including the most wildly used Lymph2Cx 20-gene assay,[38] have been applied in research studies and clinical trials,[4,39-45] although a large gene panel (145 genes) was also achievable for the NanoString nCounter system.[46] COO determined by Lymph2Cx 20-gene assay either exhibited high concordance with GEP-determined COO or showed significant prognostic value in 4 retrospective studies[47-50] and a clinical trial,[51] but not in 2 clinical trials[52] and 1 retrospective study.[53]

Reverse transcriptase–multiplex ligation-dependent probe amplification, which ligates the left and right probes annealed to cDNA target sequences, permitting amplification of specific genes,[54] is another type of assay that has been applied for DLBCL-COO classification based on expression of 14 or 21 genes.[55,56] This method is sensitive and cost-effective without using a dedicated platform but has relatively poor dynamic range and is unable to include some COO-specific genes.[55]

DLBCL outcome predictors that link GEP signatures directly to clinical outcome instead of COO have also been developed,[2,3,57,58] but the reproducibility between different studies was poor, and the predictive value for therapies other than the standard treatment is uncertain. In contrast, COO classification with underlying biology basis[9] also have predictive values for novel therapies, as demonstrated in phase 1/2 and 2/3 clinical trials.[6-8,10,11] However, recent clinical trials for adding ibrutinib (phase 3[36]) and bortezomib (phases 2[59] and 3[60]) to the standard R-CHOP in previously untreated ABC (by Hans algorithm and HTG EdgeSeq[36] or by Illumina DASL assay[60]) or non-GC (by Hans algorithm and Nanostring Lymph2Cx assay[59]) DLBCL patients failed to show improved clinical outcome.

To better classify DLBCL biologically guiding therapeutic clinical trials, genetic alteration signatures have been explored to subtype DLBCL in large numbers of patients, as genetic upstream of the oncogenic biology in DLBCL can define the response to novel targeted therapies. Schmitz et al[61] used a GenClass algorithm, and Chapuy et al[62] used an nonnegative matrix factorization (NMF) consensus clustering algorithm to analyze high-content genetic data of 574 and 304 patients, respectively, and uncovered genetically distinct subtypes within or independent of COO subtypes, most of which demonstrated robust prognostic significance and potential therapeutic relevance.[61,62] However, the pathogenic driver roles of many mutations in signatures vary or have not been validated,[63,64] and how to accurately assign a genetic subtype to new individual patients at presentation in real time is less clear than the current COO classification. In a phase 3 GOYA study (NCT01287741),[43] approximation of EZB, BN2, N1, and MCD subtypes based on presence of subtype founder gene alterations in targeted next-generation sequencing (NGS) data of 465 genes did not find prognostic effect, whereas clusters (C) C2, C3, and C5 identified by applying NMF consensus clustering to the study cohort showed poorer prognosis compared with C0, C1, and C4 clusters. In another prospective study from the LNH03B LYSA (Lymphoma Study Association) clinical trials with targeted NGS of 34 key genes and genomic copy number variation analysis, none of the genetic subtypes identified by the GenClass algorithm or NMF consensus clustering showed prognostic significance.[65] The inconsistent prognostic values could result from the highly

variable sequencing panels and NGS data quality in different studies, inaccurate subtyping, and the clinical heterogeneity within defined genetic subtypes underscored by phenotypic biologic (eg, MYC/BCL2 expression[66]) heterogeneity arising from many other underlying mechanisms, for example, epigenetic deregulation and genetic alterations in noncoding regions.[67] In fact, in the cohort of Schmitz et al, MCD patients with *MYD88/CD79B* double mutations had better survival compared with other MCD patients,[66] and the EZB subtype has been further divided into the unfavorable EZB-MYC$^+$ and favorable EZB-MYC$^-$ subtypes recently by a LymphGen algorithm.[68] A LymphGen webtool has been public accessible and able to assign genetic subtypes to patients if the input is from a cohort but not if from only 1 patient.

Based on these previous studies, we hypothesized that combined high-throughput genetic and gene expression signature analysis may improve the DLBCL classification for prognostic stratification and therapeutic implication. To be clinically applicable, fast and economical assays on FFPE samples that provide both genetic and expression data with low sample input are needed. We therefore implemented targeted RNA sequencing (RNA-Seq) of 1408 genes with NGS technology that simultaneously sequences and quantitates expressed mRNA molecules in a single assay. Artificial intelligence (AI) was implemented to build predictive models based on both genetic and gene expression data of a large number of DLBCL FFPE samples. The robustness of the predictive models was tested in validation cohorts supporting our hypothesis.

Patients and methods

Patients

RNA-seq was performed for 444 patients with de novo DLBCL diagnosed in 1998 to 2008 treated with R-CHOP at 22 medical centers. Cases were organized for retrospective studies as part of the DLBCL Consortium Program,[69] which has been approved by the institutional review board of each participating medical center and conducted in accordance with the Declaration of Helsinki. Patients with transformed DLBCL, primary mediastinal large B-cell lymphoma, primary central nervous system DLBCL, or primary cutaneous DLBCL have been excluded. Molecular characterization of the study cohort has been previously summarized.[70,71] Fluorescence in situ hybridization identified 12 of 293 cases as high-grade B-cell lymphoma with *MYC* and *BCL2* and/or *BCL6* rearrangements (7 *MYC*/*BCL2* double/triple-hit and 5 *MYC*/*BCL6* double-hit cases).

Data for 418 cases were further analyzed after data quality control. GEP was performed in 366 of the 418 patients using Affymetrix GeneChip Human Genome U133 Plus 2.0 (deposited in Gene Expression Omnibus GSE#31312).[24] Using a Bayesian model, 172, 160, and 34 cases were determined as GCB, ABC, and unclassified DLBCL, respectively. For the 34 GEP-unclassified cases, the Visco-Young IHC algorithm[24] was applied, which assigned 15 cases to GCB and 19 cases to ABC. For the other 52 cases in which GEP was not performed, the Visco-Young algorithm classified 22 cases as GCB and 23 cases as ABC.

To further validate the COO model, 60 independent DLBCL samples were obtained and classified into ABC/GCB subtypes using the Lymph2Cx NanoString nCounter assay according to the manufacturer's instructions.

GEP analysis

Raw RNA-Seq and Affymetrix GEP data were preprocessed and normalized by robust multichip average using the R package (version 1.65.1).[72] Two-class unpaired significance analysis of microarrays were performed to identify significantly differentially expressed genes (DEGs) between the 2 groups.[73] Gene expression data were analyzed via CLUSTER software using the average linkage metric and then displayed by JAVA TREEVIEW (https://www.java.com/en).[74]

RNA library construction and sequencing

The Agencourt FormaPure Total 96-Prep Kit was used to extract both DNA and RNA from the same FFPE tissue lysates using an automated KingFisher Flex and protocols as recommended by each manufacturer. Samples were selectively enriched for 1408 cancer-associated genes using reagents provided in an Illumina TruSight RNA Pan-Cancer Panel. The cDNA was generated from the cleaved RNA fragments using random primers during the first- and second-strand synthesis. Then, sequencing adapters were ligated to the resulting double-stranded cDNA fragments. The coding regions of expressed genes were captured from this library using sequence-specific probes to create the final library. Sequencing was performed on an Illumina NextSeq 550 System platform. Ten million reads per sample in a single run was required. The read length was 2 × 150 bp. The sequencing depth was 10× to 1739×, with a median of 41×. An expression profile was generated from the sequencing coverage profile of each individual sample using Cufflinks. Expression levels were measured using fragments per kilobase of transcript per million and further normalized using the B-cell PAX5 RNA expression levels to adjust for variability in the percentage of DLBC cells in samples.

Alignment of sequencing data and variant calling were performed with the DRAGEN Somatic Pipeline (Illumina) using tumor-only analysis against the GRCh37 reference genome to identify 2 classes of mutations: single nucleotide variants and indels. Tumor samples were analyzed without a matching normal.

DLBCL COO classification and clinical risk prediction modeling

To build robust DLBCL classification models, we randomly selected 60% of cases to fit (train) the model and then validated using the remaining 40% (validation set). Sixty independent DLBCL samples classified by Nanostring Lymph2Cx assay were used as a second validation set.

First, univariate significance tests were used to screen the large number of variables. Normalized RNA expression data and mutation data were included as variants to build a classification model. For interpretability and simplicity, we divided the gene expression values into 4 or 10 equal parts using the quartiles (Q1, Q2, and Q3) and deciles and selected mutation data of 39 highly recurrent genes that had mutations in at least 10 patients. Fisher's exact test was used after discretizing RNA expressions using their quartiles, and 228 variables were statistically significant with $P < .01$. After adjusting for multiple hypothesis testing using Benjamini-Hochberg's method and setting the cutoff for false discovery rate (FDR) at 0.01, statistically significant variables were narrowed down to 129. Finally, setting the cutoff for FDR

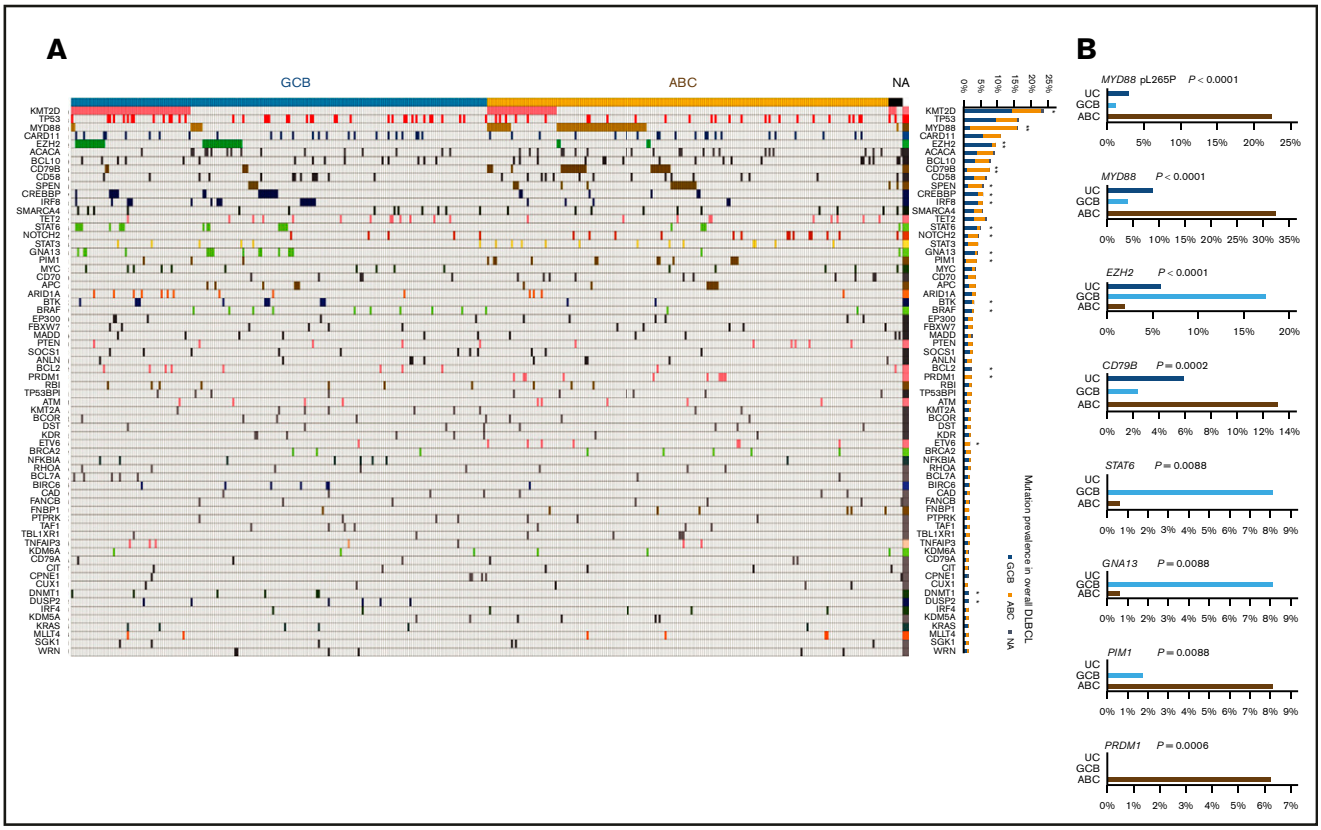

Figure 1. Case distribution and prevalence of gene mutations detected by RNA-seq in GCB and ABC subtypes of DLBCL. (A) Heatmap for distribution of gene mutations in GCB/ABC subtypes of DLBCL. Only genes mutated in ≥6 patients are shown. Each column is for each patient, and each row is for each gene. Frequency (prevalence) of mutations in overall DLBCL is on the right. Genes with significantly differential prevalence in GCB and ABC subtypes (determined by Affymetrix and/or IHC) are marked by asterisks. (B) Differential prevalence of mutations in DLBCL COO subtypes classified by gene expression profiling. Only the most significant genes are shown. UC, unclassified.

at 0.0001, 48 variables were selected with either small adjusted *P* values or high area under the receiver operating curve (AUC).

We selected 252 DLBCLs with high confidence COO assignment to develop risk stratification models directly correlating with survival. We randomly selected 60% (152) of subjects as the training set to fit the model and tested the performance in the remaining 40% (100) patients. Kaplan-Meier and Cox proportional hazards (CPH) analysis was used to identify variables with significant prognostic impact.

Multiple statistical approaches were tested for modeling performance, and models built through deep learning techniques[75,76] were most predictive and robust. We used autoencoders for nonlinear transformations of autoencoded features into 2-dimensional latent space. Logistic regression and CPH models were used for building the COO model and clinical risk models, respectively. A flowchart of the study is provided in supplemental Figure 1.

Results

Mutation spectrum, GCB/ABC association, and prognostic significance in DLBCL

In 418 patients, RNA-Seq data fulfilled the quality control criteria (supplemental Table 1) and were further analyzed. In total, 2207 nonsynonymous mutations occurred in 598 genes in 412 patients. In the study cohort, each patient had 0 to 30 genes harboring mutations (median, 4 mutated genes); 322 genes had mutations in at least 2 patients. Figure 1A shows the case distribution of mutations in 66 genes occurred in at least 6 patients. The corresponding mutation and clinical data are in the supplemental Data. The clinical features of the 418 patients are summarized in Table 1.

Mutation profile was compared between GCB and ABC subtypes classified by GEP and/or IHC (GCB, n = 209; ABC, n = 202). Mutations in *EZH2* ($P < .0001$), *KMT2D* (*MLL2*), *CREBBP*, *IRF8*, *STAT6*, *GNA13*, *BTK*, *BRAF*, *BCL2*, *DNMT1*, and *DUSP2* were significantly more frequent in GCB than in ABC, whereas mutations in *MYD88* ($P < .0001$), *CD79B* ($P < .0001$), and *SPEN*, *PIM1*, *PRDM1*, *ETV6*, and *NOTCH2* (borderline $P = .054$) were significantly more frequent in ABC than in GCB (Fisher's exact test; asterisks for significant genes in Figure 1A). The majority (69%) of *MYD88* mutations in ABC were pL273P (L265P), whereas almost half of *MYD88* mutations in GCB were pS219C.

Comparisons between GEP-classified GCB (n = 172) and ABC (n = 160) cases showed largely similar results (top significant genes are shown in Figure 1B), except that the associations of *NOTCH2* with ABC and *DUSP2* mutations with GCB became insignificant, and additionally *BIRC6* mutation and *IRF4* mutation showed significant association with GCB and ABC subtype, respectively. In

Table 1. Clinical features of the overall study cohort and GCB and ABC subtypes of DLBCL newly defined in the current study

	Overall, n (%)	GCB, n (%)	ABC, n (%)	GCB vs ABC, *P*
Patients	418 (100)	202 (100)	216 (100)	
Sex				
Male	229 (54.8)	110 (54.5)	119 (55.1)	.92
Female	189 (45.2)	92 (45.5)	97 (44.9)	
Age, y				
≤60	178 (42.6)	100 (49.5)	78 (36.1)	**.0075**
>60	240 (57.4)	102 (50.5)	138 (63.9)	
Stage of disease				
I-II	185 (46.0)	106 (54.6)	79 (38.0)	**.0009**
III-IV	217 (54.0)	88 (45.4)	129 (62.0)	
Serum LDH level				
Normal	144 (37.0)	80 (42.6)	64 (31.8)	**.036**
Elevated	245 (63.0)	108 (57.4)	137 (68.2)	
ECOG performance status				
0-1	313 (82.6)	154 (86.0)	159 (79.5)	.10
≥2	66 (17.4)	25 (14.0)	41 (20.5)	
No. of extranodal sites involved				
0-1	295 (74.3)	145 (76.3)	150 (72.5)	.42
≥2	102 (25.7)	45 (23.7)	57 (27.5)	
IPI risk group				
0-2	246 (60.9)	133 (68.9)	113 (53.6)	**.0022**
3-5	158 (39.1)	60 (31.1)	98 (46.4)	
B-symptoms				
Absence	267 (66.8)	141 (73.8)	126 (60.3)	**.0042**
Presence	133 (33.3)	50 (26.2)	83 (39.7)	
Tumor size, cm				
<5	189 (58.9)	91 (59.5)	98 (58.3)	.91
≥5	132 (41.1)	62 (40.5)	70 (41.7)	
COO by Affymetrix GEP				
GCB	172 (47.0)	149 (86.1)	23 (11.9)	**<.0001**
ABC	160 (43.7)	8 (4.6)	152 (78.9)	
UC	34 (9.3)	16 (8.7)	18 (9.3)	
COO by GEP and IHC				
GCB	209 (50.9)	180 (90.5)	29 (13.7)	**<.0001**
ABC	202 (49.1)	19 (9.5)	183 (86.3)	

Significant *P* values are in boldface.
ECOG, Eastern Cooperative Oncology Group; LDH, lactate dehydrogenase; IPI, International Prognostic Index.

addition, the 34 GEP-unclassified cases had higher frequencies of *CREBBP* and *BRAF* mutations than both GCB and ABC subtypes.

Mutation status of each gene was analyzed for prognostic significance. Table 2 lists frequently mutated genes with significant mutational effects on overall survival (OS) by univariate analysis. Among genes with mutations occurring in at least 9 patients, *TP53*, *TET2*, *KMT2D* (in overall cohort, $P = .0005$, .011, and .012, respectively), *NOTCH2* (in GCB, $P = .005$), and *ATM* (in ABC, $P = .003$) mutations showed significantly adverse effects, whereas *EZH2* and *GNA13* mutations genes showed significantly favorable effects ($P = .007$ and .047, respectively).

Development and validation of the NGS-COO classification model

RNA-Seq gene expression (supplemental Data), gene fusion, and mutation data were used to develop a model for DLBCL-COO classification in the training set. Fisher's exact test and multiple hypothesis testing adjustment were used to identify RNA-Seq variables showing significant difference between GCB and ABC subtypes. DEGs between GEP-classified GCB and ABC subtypes are visualized in Figure 2A (FDR < 0.1, fold change ≥ 1.42). Finally, the top 48 variables (Table 3; Figure 2B) that were significantly differed between GCB and ABC subtypes with FDR < 0.0001 or

Table 2. List of genes with >2% mutational prevalence and significant impact on OS rate in DLBCL

		In DLBCL		In GCB		In ABC	
Gene	**Effect on OS**	**Mutation frequency, %**	***P* for OS**	**Mutation frequency, %**	***P* for OS**	**Mutation frequency, %**	***P* for OS**
KMT2D	Unfavorable	23.7	.012	28.5	.005	17.5	—
TP53	Unfavorable	16.3	.0005	19.8	.024	13.1	.034
EZH2	Favorable	9.3	.007	17.4	.04	1.9	—
TET2	Unfavorable	5.5	.011	6.4	.011	4.4	—
NOTCH2	Unfavorable	4.5	(.061)	2.9	.005	6.9	—
GNA13	Favorable	4.1	.047	8.1	(.09)	0.6	—
ATM	Unfavorable	2.2	(.085)	1.7	—	2.5	.003

The DLBCL group had 418 patients. The GCB group, determined by gene-expression profiling, had 172 patients. The ABC group, determined by gene-expression profiling, had 160 patients. The impact on OS was based on univariate analysis for each gene. Marginal *P* values are in the parentheses. Dashes indicate not prognostic.

high AUC were chosen to build a new classification model for RNA-Seq data, including 2 genes (*MYD88* and *EZH2*)′s mutation status and 46 genes′ RNA expression levels.

Several statistical models were built on the 48 variables in the training set (without knowing classification) and then tested in the validation sets. The COO model based on autoencoder, an unsupervised deep learning technique, showed the best performance. An autoencoder neural network was built with 5 hidden layers.[75,76] The first 2 layers and the last 2 layers each had 100 neurons; the middle layer (bottleneck) had 2 neurons, which captured latent (unobserved) features of the data. The values of these 2 neurons formed a low-dimensional (2) representation of the data; that is, it aggregated the 48 variables into 2 latent features. The top 7 contributing variables to the latent features were *MYD88* mutation, *EZH2* mutation, *RASGRF1* expression, *MYBL1* expression, *S1PR2* expression, *SSBP2* expression, and *IRF4* expression. Based on the latent features, a logistic regression model was built for GCB/ABC classification (named as NGS-COO classifier). As shown in Figure 3A, the autoencoder transformed the high-dimensional data into a 2-dimensional space where the 2 subtypes were easily separable (linearly) roughly with a diagonal line from (−1, −1) to (1, 1).

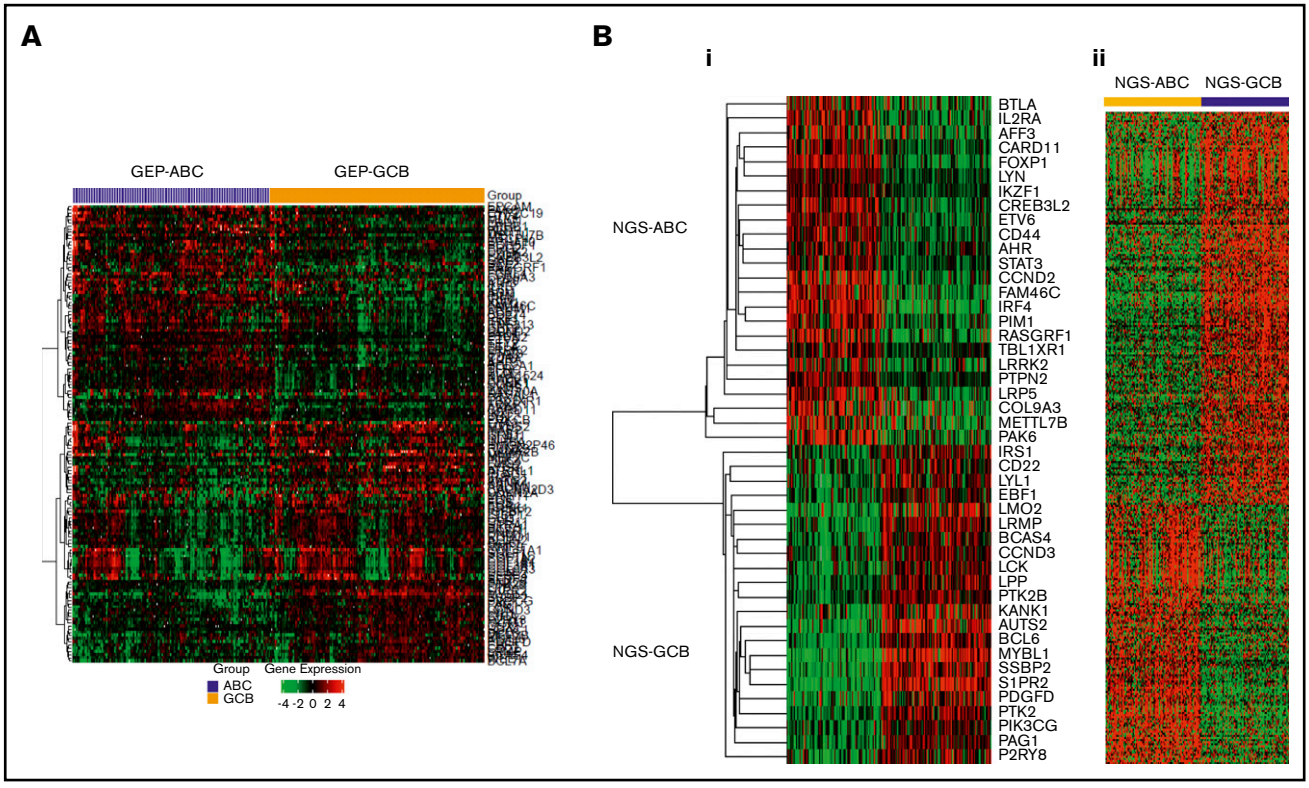

Figure 2. Heatmaps for significant differential gene expression between GCB and ABC subtypes classified by Affymetrix GeneChip or RNA-seq. (A) RNA-seq expression data (significant genes with FDR < 0.10 and fold change ≥ 1.42) of previous GCB/ABC subtypes classified by Affymetrix GeneChip DNA microarray data. (Bi) RNA-seq expression data (top 46 genes selected for the new NGS-COO classifier) of the new GCB/ABC groups. (Bii) Affymetrix GeneChip microarray data of the new GCB/ABC groups.

Table 3. List of 48 variables (46 for gene expression level and 2 for gene mutation status) in the DLBCL NGS-COO classifier

AFF3	*AHR*	*AUTS2*	*BCAS4*	*BCL6*	*BTLA*
CARD11	*CCND2*	*CCND3*	*CD22*	*CD44*	*COL9A3*
CREB3L2	*EBF1*	*ETV6*	*FAM46C*	*FOXP1*	*IKZF1*
IL2RA	*IRF4*	*IRS1*	*KANK1*	*LCK*	*LMO2*
LPP	*LRMP*	*LRP5*	*LRRK2*	*LYL1*	*LYN*
METTL7B	*EZH1* mutation	*MYD88* mutation	*MYBL1*	*P2RY8*	*PAG1*
PAK6	*PDGFD*	*PIK3CG*	*PIM1*	*PTK2*	*PTK2B*
PTPN2	*RASGRF1*	*S1PR2*	*SSBP2*	*STAT3*	*TBL1XR1*

The NGS-COO classifier developed from the training set was then applied to the validation set. A probability of scoring was generated for each case. Approximately 30% of the cases had a score between 0.5 and 0.75, indicating low confidence for classification. For the remaining 70% with high confidence for assigning to 1 of the 2 subtypes (probability of 0.8 or higher), the ABC vs GCB classification showed sensitivity and specificity of 96% and 97% for classification in the validation set. The accuracy/concordance rate with previous GCB/ABC classification was 95.6%. The corresponding AUC was 96.2%.

In the training and validation sets, in total, 216 cases were determined as the ABC subtype and 202 cases as the GCB subtype. Differential expression of the 46 genes constituting the NGS-COO classifier in the study cohort is visualized in Figure 2B. The new GCB/ABC cases were also associated with 1319 significant DEGs with FDR $<$ 0.0001 in GEP analysis using our previous Affymetrix GeneChip DNA microarray data (Figure 2B) and multiple biomarkers characterized in previous studies by our Consortium program (supplemental Table 2).

To further evaluate the performance of the NGS-COO classification model, we applied the same approach to 60 independent cases as an external validation cohort. Our NGS-COO model showed sensitivity and specificity of 96% and 97%, respectively, with the previous COO classification by the NanoString Lymph2Cx assay. The concordance rate was 92.9%. The corresponding AUC was 95.7%. As shown in Figure 3B-C, the pattern of separation by the autoencoder was similar between training, validation, and independent sets. They all showed separation between ABC and GCB with a diagonal line from (−1, −1) to (1,1), although the independent 60 cases were collected from a completely different set of samples and the sequencing was performed separately.

The performance of our NGS-COO classifier was also evaluated by correlating with survival outcomes. Although the autoencoder was only trained for COO classification in the training set, the NGS-COO classifier was significantly associated with OS and progression-free survival (PFS) in DLBCL, similar to the previous COO classification (Figure 4A-C). The relative risk of the new ABC compared with the new GCB group was 1.53. The prognostic significance was slightly improved if comparing within high-confidence cases only (risk for OS, 1.81, $P = .007$; risk for PFS, 1.77, $P = .0046$).

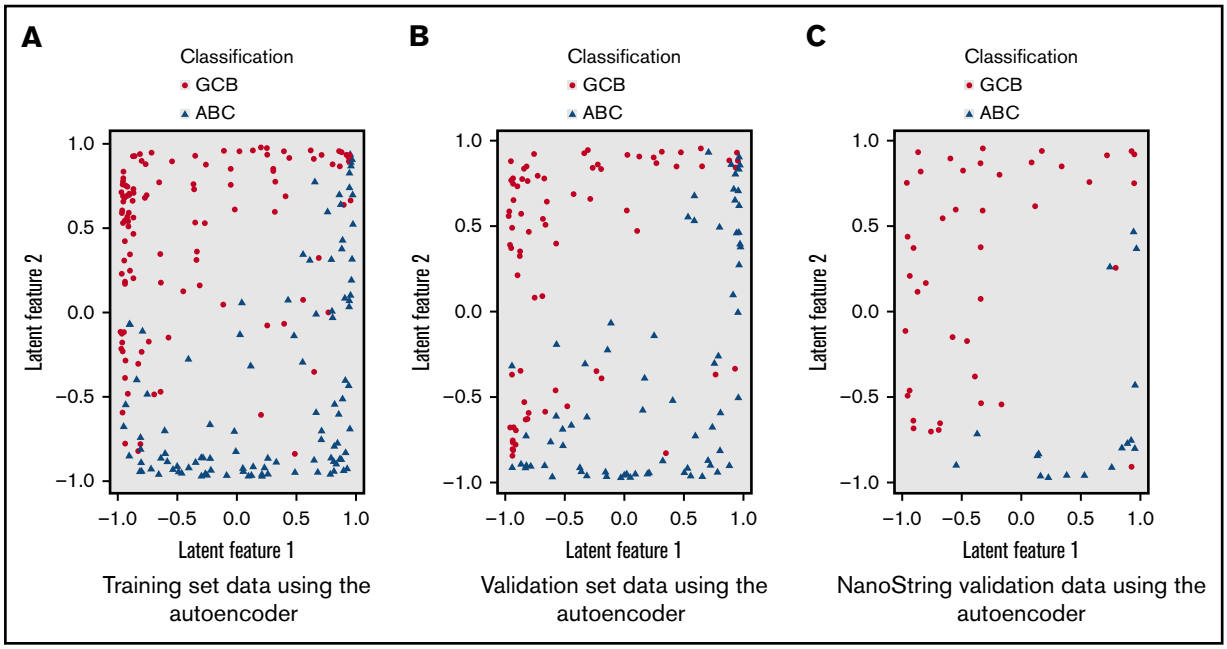

Figure 3. Two-dimensional representation of the training and validation set data using the autoencoder. (A) Training set data using the autoencoder. (B) Validation set data using the autoencoder. (C) NanoString validation data using the autoencoder.

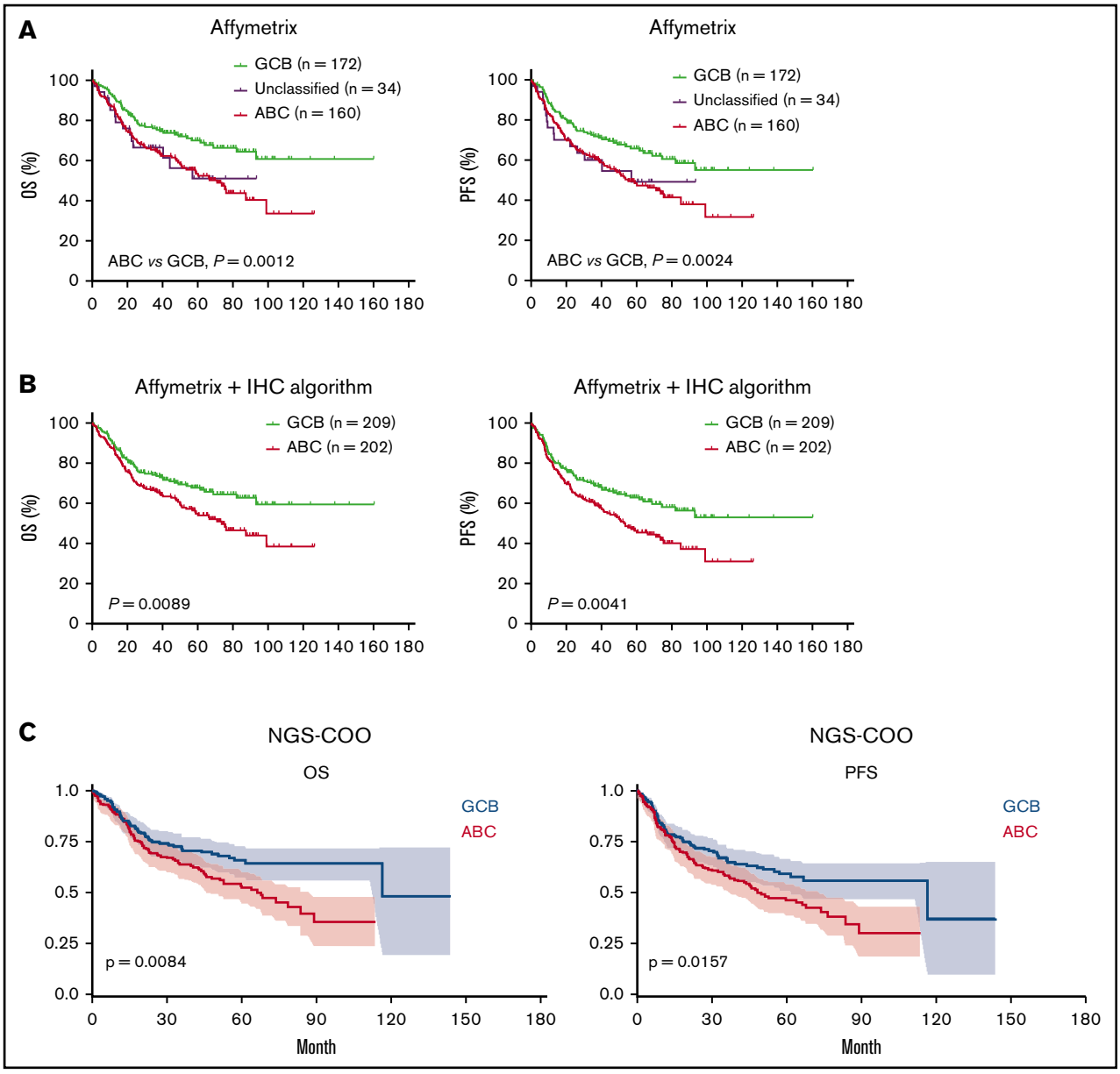

Figure 4. Survival curves for GCB vs ABC subtypes of DLBCL defined by previous classification methods and the new NGS-COO classifier. (A) Three subtypes defined by a 100-gene-classifier for gene-expression profiled cases using Affymetrix GeneChip. (B) GCB and ABC subtypes defined by a 100-gene-classifier and the Visco-Young IHC algorithm as described in "Patients and methods." (C) GCB and ABC subtypes defined by the new NGS-COO classifier.

Development of prognostic models for DLBCL risk stratification

To build robust prognostic models aggregating small contributions of a large number of variables directly to patient survival, we used a similar procedure and the AI method to develop models in the training set and test the performance in the validation set based on both gene expression and genetic variables plus 2 additional factors: age and sex of patients. We first screened for significant variables using Kaplan-Meier and CPH for OS in the training set. Although 61 variables showed significant prognostic effects by log-rank test and 110 variables by CPH regression ($P < .05$), only the *TP53* mutation remained statistically significant after adjusting for multiple hypothesis testing (FDR < 0.0001). Therefore, we selected 57 variables with the top 2% AUC values or $P < .01$ (either based on log-rank test or CPH; Table 4).

We used a similar neural network architecture as described for COO modeling and again included 2 neurons in the bottleneck layer to reduce the data into 2 dimensions (latent features). The top 7 variables contributing to the 2 latent features are age >60, *TP53* mutation, *CARD11* expression, *BCL6* expression, *MALAT1* expression, *RABEP1* expression, and *BCORL1* expression. A simple CPH model was built based on the 2 latent features obtained from the autoencoder (which are nonlinear combinations of the 57 variables) and provided a risk score (NGS-OS score) for each case,

Table 4. List of 57 variables (55 for gene expression level and 2 for gene mutation status) selected for building the NGS-OS risk model

AFF3	Age >60	*ASPSCR1*	*BCL2*	*BCL6*	*BCORL1*
BHLHE22	*BTK*	*CARD11*	*CCND2*	*CD58*	*CHEK2*
CIT	*CREB3L2*	*DST*	*ETS1*	*EYA2*	*FANCF*
FZD6	*GAS5*	*HMGA1*	*HOXA9*	*IRF4*	*KDM5C*
KLK2	*LFNG*	*LMO2*	*MACROD1*	*MALAT1*	*MEF2B/MEF2BNB-MEF2B*
MFNG	*MLLT4*	*MTCP1*	*TET2* mutation	*TP53* mutation	*MYC*
PIM1	*POLD1*	*PPP3CA*	*RABEP1*	*RAD51B*	*RBM6*
RECQL4	*RHBDF2*	*RLTPR*	*RTEL1-TNFRSF6B*	*SMAD3*	*SPTBN1*
SRRM3	*ST6GAL1*	*SULF1*	*SYP*	*TEAD2*	*TFAP2A*
TGFBR3	*U2AF2*	*ZIC2*			

which was normalized to be between 0 (lowest risk) and 100 (highest risk). As shown in Figure 5A, we divided the training set into 3 equal subgroups based on the NGS-OS risk score and found the high-risk group had strikingly poorer survival than the low- and intermediate-risk groups ($P < .0001$). We then applied the NGS-OS model into the validation set and stratified patients using the same NGS-OS risk score cutoffs established in the training set and found that 3 resulting risk groups in the validation set showed incremental survival rates. The relative OS risk for the 3 subgroups was roughly 1, 4, and 9.

We followed a similar procedure to build a CPH model for PFS with 50 selected variables based on a 2-dimensional feature set obtained from an autoencoder (Table 5). The top 7 variables contributing to the model are *TP53* mutation, *CDK8* expression, *LMO2* expression, *BCR* expression, *TGFBR2* expression, *CHD2* expression, and *ETS1* expression. Although 24 variables are shared by the NGS-OS and NGS-PFS models, there are only 7 genes (*AFF3*, *BCL6*, *CARD11*, *CCND2*, *IRF4*, *LMO2*, and *PIM1*) shared by the NGS-COO and NGS-OS models and 5 genes (*AFF3, BTLA, CREB3L2, FOXP1,* and *LMO2*) shared by the NGS-COO and NGS-PFS models.

Similar with the NGS-OS risk scores, NGS-PFS risk scores identified one third of the training set and 30% of the validation set as high-risk patients (Figure 5B). The relative risk for the low-, intermediate-, and high-risk groups in the validation sets was roughly 1, 2, and 4, respectively.

Discussion

In this study, we developed novel DLBCL classification models based on both genetic and transcriptional variables derived from comprehensive RNA-Seq annotation and quantitative data. Molecular classification methods based on tumor biology can be categorized according to whether the model is based on normal or abnormal signatures and whether the measure is at the DNA (genetic), RNA (transcriptional), or protein level (summarized in the visual abstract according to the literature[1-3,14,17-24,57,58,61,62,68,77,78]). The mandatory COO classification for DLBCL with significant prognostic and therapeutic prediction values is originally based on unaltered normal B-cell GEP signatures and currently assayed by protein IHC algorithms in clinical practice, whereas the recently developed DLBCL genetic subtyping defines subtypes with shared genetic abnormalities based on co-occurring genetic alterations or co-ordinate genetic signatures. Therefore, genetic subtypes, such as the MCD/C5 subtype in ABC-DLBCL and the C3/EZB subtype in GCB-DLBCL,[61,79] reduce the heterogeneity in COO subtypes with respect to pathogenic mechanisms (potentially also response to targeted therapies). However, the functional consequences of different genetic alterations defining a genetic subtype may vary, and pathogenic subtyping can also be achieved with phenotypic gene expression signatures.[3] Different from genetic subtyping that assigned *MYC*/*BCL2* double-hit lymphoma into multiple genetic subtypes (visual abstract),[61,62] molecular high-grade (MHG) GEP signature or double-hit transcriptomic gene-expression signature (DHITsig) defined a distinct MHG or DHITsig-positive (DHITsig-pos) subgroup with poor prognosis in GCB-DLBCL.[77,78] Only 36% of MHG and 52% of DHITsig-pos cases had *MYC*/*BCL2* genetic double hit[60,77,78]; certain mutations and the EZB genetic subtype were enriched (but not exclusively or inclusively; overlapping percentages shown in visual abstract) in the MHG/DHITsig-pos DLBCL subgroup. In contrast to the COO classification and nuclear factor κB–activating genetic mutations that failed to predict clinical outcome of bortezomib,[60] MHG GEP signature identified cases showing improved PFS with the addition of bortezomib to standard R-CHOP therapy ($P = .08$).[77] Therefore, both genetic and phenotypic variables have advantages and disadvantages, and a combinational approach may better correlate DLBCL biology to therapeutic vulnerability and clinical outcome.

Our results demonstrated that both the NGS-COO classifier and NGS survival predictors were robust, and AI was able to assign COO/risk scores to new DLBCL cases (patients in the validation sets). Our NGS-COO classifier shared 8 genes with the 27-gene predictor by Wright et al (*BCL6*, *CCND2*, *ETV6*, *IRF4*, *LMO2*, *LRMP*, *MYBL1*, and *PIM1*),[31] 8 genes with the 20-gene DLBCL Automatic classifier by Barrans et al (*BCL6*, *CCND2*, *ETV6*, *FOXP1*, *IRF4, LMO2, LRMP*, and *PIM1*),[30] 7 genes with the 14-gene-qNPA assay (*BCL6*, *CCND2*, *IRF4*, *LMO2, LRMP*, *MYBL1* and *PIM1*),[35] and 3 genes with the NanoString Lymph2Cx assay (*CREB3L2*, *MYBL1*, and *S1PR2*).[38] Seven of the total 11 common genes (*BCL6*, *CCND2*, *CREB3L2, FOXP1, IRF4*, *LMO2*, and *PIM1*) are also shared by our NGS survival predictors, consistent with the association of COO with clinical outcome. The NGS-OS/PFS risk predictors had more significant *P* values in prognostic analysis than the NGS-COO classifier in the same patient cohort, suggesting that COO is only one of the biological contributors to DLBCL clinical outcome. However, the performance of NGS-OS/PFS risk predictors for other therapies is unknown. Different from previous COO/prognostic models, we integrated genetic abnormalities: *MYD88* and *EZH2* mutations in the NGS-COO classification

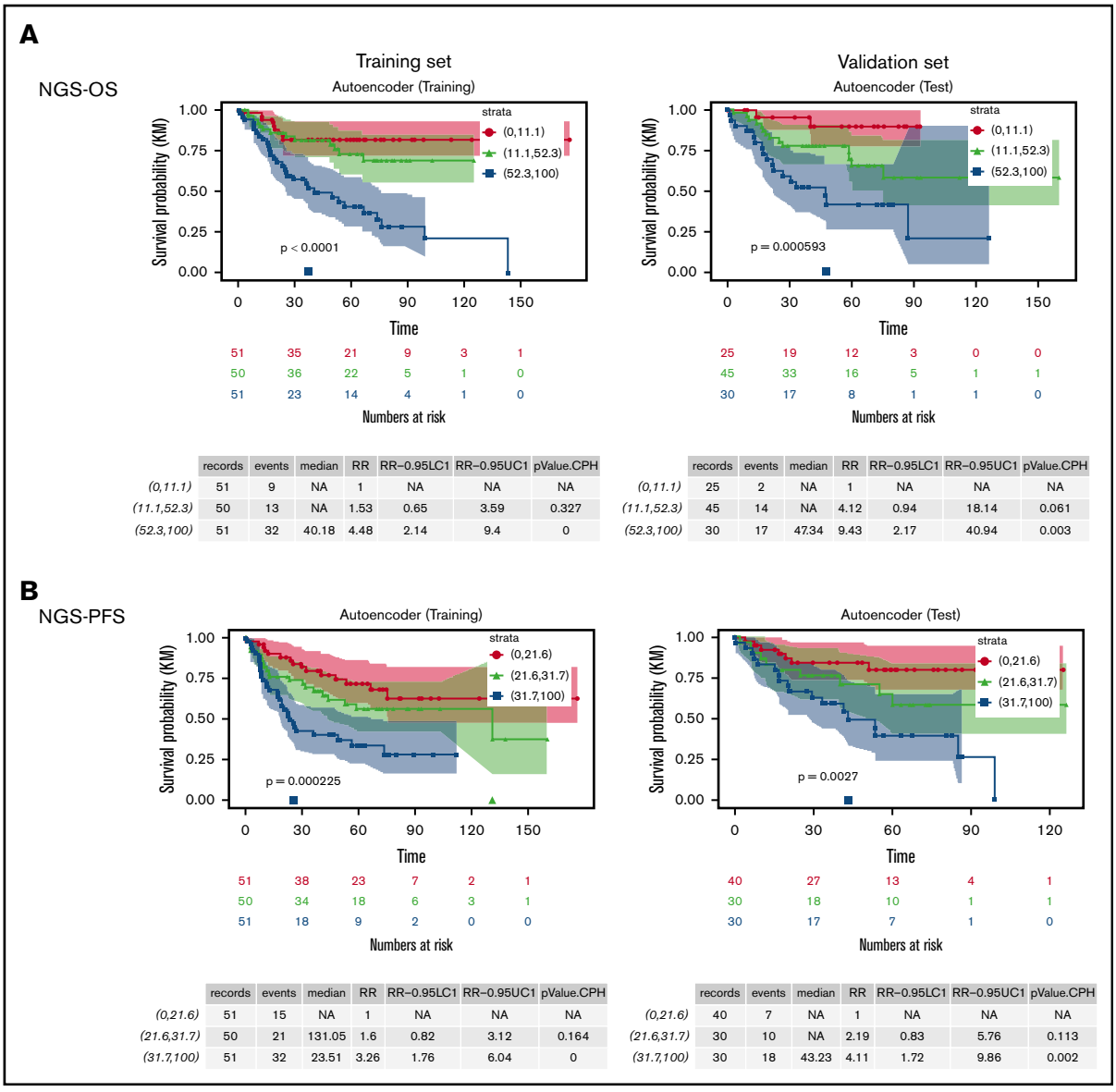

	records	events	median	RR	RR−0.95LC1	RR−0.95UC1	pValue.CPH
(0,11.1)	51	9	NA	1	NA	NA	NA
(11.1,52.3)	50	13	NA	1.53	0.65	3.59	0.327
(52.3,100)	51	32	40.18	4.48	2.14	9.4	0

	records	events	median	RR	RR−0.95LC1	RR−0.95UC1	pValue.CPH
(0,11.1)	25	2	NA	1	NA	NA	NA
(11.1,52.3)	45	14	NA	4.12	0.94	18.14	0.061
(52.3,100)	30	17	47.34	9.43	2.17	40.94	0.003

	records	events	median	RR	RR−0.95LC1	RR−0.95UC1	pValue.CPH
(0,21.6)	51	15	NA	1	NA	NA	NA
(21.6,31.7)	50	21	131.05	1.6	0.82	3.12	0.164
(31.7,100)	51	32	23.51	3.26	1.76	6.04	0

	records	events	median	RR	RR−0.95LC1	RR−0.95UC1	pValue.CPH
(0,21.6)	40	7	NA	1	NA	NA	NA
(21.6,31.7)	30	10	NA	2.19	0.83	5.76	0.113
(31.7,100)	30	18	43.23	4.11	1.72	9.86	0.002

Figure 5. Risk stratification of DLBCL patients by the new NGS-survival risk scores from Cox proportional hazards models based on two latent features of the data obtained from the autoencoders. (A) OS curves of 3 risk groups defined by the NGS-OS risk scores. (B) PFS curves of 3 risk groups defined by the NGS-PFS risk scores.

model, *TP53* and *TET2* mutations in the NGS-OS risk model, and *TP53* mutation in the NGS-PFS model. Future studies may reveal whether our models can improve the practical significance of DLBCL prediction models by including both GEP and genetic features.

The high-throughput RNA-Seq assays developed in this study using an NGS benchtop sequencer with approximately 3-day turnaround time have important practical implications. Although targeted NGS platforms have been implemented in the clinic to aid in diagnosis and therapeutic decisions,[80] and AI is emerging as an efficient tool in health care for large data processing and sophisticate model construction,[76,81] currently no NGS panels and AI implementation have been developed for lymphoma diagnosis and management. Our study supports the reliability and practicality of using targeted NGS along with AI in generating clinically useful objective information. Compared with current IHC assays, DNA microarrays, and other GEP analysis techniques used for DLBCL COO classification, targeted RNA-Seq has a balanced advantage of genome-wide coverage, dynamic range of quantification, reproducibility, high throughput, and accuracy, as well as high sensitivity, automation, affordability, short assay time, and flexibility.[82] As RNA-seq has become less costly and been integrated into clinical practice,[80] we expect that the generated RNA-seq data will be used not only to answer the COO and prognostic questions but also other diagnostic and clinical questions impacting clinical decisions, such as predicting clinical responses to novel therapies in clinic and in future prospective or retrospective studies.[80,83]

In conclusion, the current proof-of-principle study demonstrates the potential utility of the targeted RNA-Seq assay for accurate and

Table 5. List of 50 variables (49 for gene expression level and *TP53* gene mutation status) selected for building the NGS-PFS risk model

AFF1	*AFF3*	*ASPSCR1*	*ATM*	*BCL2*	*BCR*
BTG2	*BTK*	*BTLA*	*CDK12*	*CDK8*	*CHD2*
CHEK2	*CIRH1A*	*CREB3L2*	*DDIT3*	*EDNRB*	*EPHB6*
ETS1	*FANCF*	*FOXP1*	*FZD6*	*GAB1*	*GAS5*
GPR34	*IQCG*	*ITGA7*	*KDM5C*	*KDSR*	*LAMA5*
LFNG	*LIFR*	*LMO2*	*MACROD1*	*MAP2K5*	*MFNG*
TP53 mutation	*MYC*	*NCSTN*	*NR6A1*	*POU2AF1*	*PRKCB*
RLTPR	*RPL22*	*SHC2*	*SMAD3*	*SPTBN1*	*ST6GAL1*
TEAD2	*TGFBR2*				

reproducible DLBCL-COO subclassification in daily clinical practice using a commercial available NGS platform; streamline analysis of high-throughput RNA-Seq data, COO assignment, and risk prediction by AI can further improve the workflow. Data portal and streamline AI integration can be further developed based on results in this study, which may provide a reliable tool for precision medicine and decision making by clinicians. However, the predictive and therapeutic values of the COO and risk stratification models developed in this large cohort of DLBCL remain to be determined in future prospective clinical studies.

Acknowledgments

This work is supported by the Cancer Prevention & Research Institute of Texas, Genomic Testing Corporative Collaboration Funds, and National Cancer Institute, National Institutes of Health grants (1R01CA233490-01A1, R01CA138688, R01CA187415, and 1RC1CA146299). K.H.Y. is also supported by The Hagemeister Lymphoma Foundation, Gundersen Foundation, and a Duke University Institutional Research grant award. The study is also partially supported by Duke Cancer Center Support Grant.

Authorship

Contribution: Z.Y.X.-M., B.X., M.A., and K.H.Y. conceived and designed the study; Z.Y.X.-M., Hongwei Zhang, B.X., M.A., and K.H.Y. performed research; Z.Y.X.-M., Hongwei Zhang, F.Z., A.T., G.B., C.V., K.D., A.C., W.T., Y.Z., E.D.H., H.Y., J.H., M.P., A.J.M.F., M.B.M., B.M.P., J.H.v.K., M.A.P., J.N.W., F.B.H., B.S., I.D.D., Hong Zhang, Y.L., B.X., M.A., and K.H.Y. provided study thought, materials, key reagents, and technology; Z.Y.X.-M., Hongwei Zhang, F.Z., A.T., G.B., C.V., K.D., A.C., W.T., Y.Z., E.D.H., H.Y., J.H., M.P., A.J.M.F., M.B.M., B.M.P., J.H.v.K., M.A.P., J.N.W., F.B.H., B.S., I.D.D., Hong Zhang, Y.L., B.X., M.A., and K.H.Y. collected and assembled the data under approved IRB and material transfer agreements; Z.Y.X.-M., Hongwei Zhang, B.X., M.A., and K.H.Y. performed data analysis and interpretation; Z.Y.X.-M., B.X., M.A., and K.H.Y. wrote the manuscript; and all authors provided final approval of the manuscript.

Conflict-of-interest disclosure: I.D.D. and M.A. are employees of Genomic Testing Corporative, LCA. K.H.Y. receives research support from Roche Molecular Diagnostics, Adaptive Biotechnologies, Gilead Sciences, Seattle Genetics, Daiichi Sankyo, Incyte Corporation, and HTG Molecular Diagnostics. The remaining authors declare no competing financial interests.

ORCID profiles: Z.Y.X.-M., 0000-0002-7615-3949; C.V., 0000-0003-2863-0883; K.D., 0000-0003-2488-435X; H.Y., 0000-0002-9630-5284; A.J.M.F., 0000-0001-9606-6124; M.B.M., 0000-0003-2041-36300000-0002-5634-2937B.M.P.B.S., 0000-0002-8102-1609; K.H.Y., 0000-0002-5755-8932.

Correspondence: Ken H. Young, Division of Hematopathology, Department of Pathology, Duke University School of Medicine, Duke University Medical Center and Cancer Institute, 40 Duke Medicine Cir, Room 265M, Box 3712, Duke South, Green Zone, Durham, NC 27710; e-mail: ken.young@duke.edu; Bing Xu, The First Affiliated Hospital of Xiamen University, 55 Zhenhai Rd, Siming District, Xiamen, Fujian 361003, China; e-mail: xubingzhangjian@126.com; and Maher Albitar, Genomic Testing Cooperative LCA, 175 Technology Dr, Irvine, CA 92618; e-mail: malbitar@genomictestingcooperative.com.

References

1. Alizadeh AA, Eisen MB, Davis RE, et al. Distinct types of diffuse large B-cell lymphoma identified by gene expression profiling. *Nature*. 2000;403(6769):503-511.
2. Lenz G, Wright G, Dave SS, et al; Lymphoma/Leukemia Molecular Profiling Project. Stromal gene signatures in large-B-cell lymphomas. *N Engl J Med*. 2008;359(22):2313-2323.
3. Rosenwald A, Wright G, Chan WC, et al; Lymphoma/Leukemia Molecular Profiling Project. The use of molecular profiling to predict survival after chemotherapy for diffuse large-B-cell lymphoma. *N Engl J Med*. 2002;346(25):1937-1947.
4. Vitolo U, Trněný M, Belada D, et al. Obinutuzumab or rituximab plus cyclophosphamide, doxorubicin, vincristine, and prednisone in previously untreated diffuse large B-cell lymphoma. *J Clin Oncol*. 2017;35(31):3529-3537.
5. Thieblemont C, Briere J, Mounier N, et al. The germinal center/activated B-cell subclassification has a prognostic impact for response to salvage therapy in relapsed/refractory diffuse large B-cell lymphoma: a bio-CORAL study. *J Clin Oncol*. 2011;29(31):4079-4087.
6. Castellino A, Chiappella A, LaPlant BR, et al. Lenalidomide plus R-CHOP21 in newly diagnosed diffuse large B-cell lymphoma (DLBCL): long-term follow-up results from a combined analysis from two phase 2 trials. *Blood Cancer J*. 2018;8(11):108.

7. Czuczman MS, Trněný M, Davies A, et al. A phase 2/3 multicenter, randomized, open-label study to compare the efficacy and safety of lenalidomide versus investigator's choice in patients with relapsed or refractory diffuse large B-cell lymphoma. *Clin Cancer Res*. 2017;23(15):4127-4137.
8. Goy A, Ramchandren R, Ghosh N, et al. Ibrutinib plus lenalidomide and rituximab has promising activity in relapsed/refractory non-germinal center B-cell-like DLBCL. *Blood*. 2019;134(13):1024-1036.
9. Wilson WH, Young RM, Schmitz R, et al. Targeting B cell receptor signaling with ibrutinib in diffuse large B cell lymphoma. *Nat Med*. 2015;21(8): 922-926.
10. Ruan J, Martin P, Furman RR, et al. Bortezomib plus CHOP-rituximab for previously untreated diffuse large B-cell lymphoma and mantle cell lymphoma. *J Clin Oncol*. 2011;29(6):690-697.
11. Herrera AF, Goy A, Mehta A, et al. Safety and activity of ibrutinib in combination with durvalumab in patients with relapsed or refractory follicular lymphoma or diffuse large B-cell lymphoma. *Am J Hematol*. 2020;95(1):18-27.
12. Schneider C, Pasqualucci L, Dalla-Favera R. Molecular pathogenesis of diffuse large B-cell lymphoma. *Semin Diagn Pathol*. 2011;28(2):167-177.
13. Davis RE, Ngo VN, Lenz G, et al. Chronic active B-cell-receptor signalling in diffuse large B-cell lymphoma. *Nature*. 2010;463(7277):88-92.
14. Hu S, Xu-Monette ZY, Tzankov A, et al. MYC/BCL2 protein coexpression contributes to the inferior survival of activated B-cell subtype of diffuse large B-cell lymphoma and demonstrates high-risk gene expression signatures: a report from The International DLBCL Rituximab-CHOP Consortium Program. *Blood*. 2013;121(20):4021-4031, quiz 4250.
15. Mai Y, Yu JJ, Bartholdy B, et al. An oxidative stress-based mechanism of doxorubicin cytotoxicity suggests new therapeutic strategies in ABC-DLBCL. *Blood*. 2016;128(24):2797-2807.
16. Swerdlow SH, Campo E, Pileri SA, et al. The 2016 revision of the World Health Organization classification of lymphoid neoplasms. *Blood*. 2016;127(20): 2375-2390.
17. Colomo L, López-Guillermo A, Perales M, et al. Clinical impact of the differentiation profile assessed by immunophenotyping in patients with diffuse large B-cell lymphoma. *Blood*. 2003;101(1):78-84.
18. Hans CP, Weisenburger DD, Greiner TC, et al. Confirmation of the molecular classification of diffuse large B-cell lymphoma by immunohistochemistry using a tissue microarray. *Blood*. 2004;103(1):275-282.
19. de Jong D, Rosenwald A, Chhanabhai M, et al; Lunenburg Lymphoma Biomarker Consortium. Immunohistochemical prognostic markers in diffuse large B-cell lymphoma: validation of tissue microarray as a prerequisite for broad clinical applications—a study from the Lunenburg Lymphoma Biomarker Consortium. *J Clin Oncol*. 2007;25(7):805-812.
20. Muris JJ, Meijer CJ, Vos W, et al. Immunohistochemical profiling based on Bcl-2, CD10 and MUM1 expression improves risk stratification in patients with primary nodal diffuse large B cell lymphoma. *J Pathol*. 2006;208(5):714-723.
21. Choi WW, Weisenburger DD, Greiner TC, et al. A new immunostain algorithm classifies diffuse large B-cell lymphoma into molecular subtypes with high accuracy. *Clin Cancer Res*. 2009;15(17):5494-5502.
22. Meyer PN, Fu K, Greiner TC, et al. Immunohistochemical methods for predicting cell of origin and survival in patients with diffuse large B-cell lymphoma treated with rituximab. *J Clin Oncol*. 2011;29(2):200-207.
23. Gutiérrez-García G, Cardesa-Salzmann T, Climent F, et al; Grup per l'Estudi dels Limfomes de Catalunya I Balears (GELCAB). Gene-expression profiling and not immunophenotypic algorithms predicts prognosis in patients with diffuse large B-cell lymphoma treated with immunochemotherapy. *Blood*. 2011;117(18):4836-4843.
24. Visco C, Li Y, Xu-Monette ZY, et al. Comprehensive gene expression profiling and immunohistochemical studies support application of immunophenotypic algorithm for molecular subtype classification in diffuse large B-cell lymphoma: a report from the International DLBCL Rituximab-CHOP Consortium Program Study [published correction appears in *Leukemia* 2014;28:980]. *Leukemia*. 2012;26(9):2103-2113.
25. Molina TJ, Canioni D, Copie-Bergman C, et al. Young patients with non-germinal center B-cell-like diffuse large B-cell lymphoma benefit from intensified chemotherapy with ACVBP plus rituximab compared with CHOP plus rituximab: analysis of data from the Groupe d'Etudes des Lymphomes de l'Adulte/ lymphoma study association phase III trial LNH 03-2B. *J Clin Oncol*. 2014;32(35):3996-4003.
26. Ott G, Ziepert M, Klapper W, et al. Immunoblastic morphology but not the immunohistochemical GCB/nonGCB classifier predicts outcome in diffuse large B-cell lymphoma in the RICOVER-60 trial of the DSHNHL. *Blood*. 2010;116(23):4916-4925.
27. Moskowitz CH, Zelenetz AD, Kewalramani T, et al. Cell of origin, germinal center versus nongerminal center, determined by immunohistochemistry on tissue microarray, does not correlate with outcome in patients with relapsed and refractory DLBCL. *Blood*. 2005;106(10):3383-3385.
28. Saad AG, Grada Z, Bishop B, et al. nCounter NanoString assay shows variable concordance with immunohistochemistry-based algorithms in classifying cases of diffuse large B-cell lymphoma according to the cell-of-origin. *Appl Immunohistochem Mol Morphol*. 2019;27(9):644-648.
29. Williams PM, Li R, Johnson NA, Wright G, Heath JD, Gascoyne RD. A novel method of amplification of FFPET-derived RNA enables accurate disease classification with microarrays. *J Mol Diagn*. 2010;12(5):680-686.
30. Barrans SL, Crouch S, Care MA, et al. Whole genome expression profiling based on paraffin embedded tissue can be used to classify diffuse large B-cell lymphoma and predict clinical outcome. *Br J Haematol*. 2012;159(4):441-453.
31. Wright G, Tan B, Rosenwald A, Hurt EH, Wiestner A, Staudt LM. A gene expression-based method to diagnose clinically distinct subgroups of diffuse large B cell lymphoma. *Proc Natl Acad Sci USA*. 2003;100(17):9991-9996.
32. Martel RR, Botros IW, Rounseville MP, et al. Multiplexed screening assay for mRNA combining nuclease protection with luminescent array detection. *Assay Drug Dev Technol*. 2002;1(1 Pt 1):61-71.
33. Qi Z, Wang L, He A, Ma-Edmonds M, Cogswell J. Evaluation and selection of a non-PCR based technology for improved gene expression profiling from clinical formalin-fixed, paraffin-embedded samples. *Bioanalysis*. 2016;8(22):2305-2316.

34. Roberts RA, Sabalos CM, LeBlanc ML, et al. Quantitative nuclease protection assay in paraffin-embedded tissue replicates prognostic microarray gene expression in diffuse large-B-cell lymphoma. *Lab Invest*. 2007;87(10):979-997.

35. Rimsza LM, Wright G, Schwartz M, et al. Accurate classification of diffuse large B-cell lymphoma into germinal center and activated B-cell subtypes using a nuclease protection assay on formalin-fixed, paraffin-embedded tissues. *Clin Cancer Res*. 2011;17(11):3727-3732.

36. Younes A, Sehn LH, Johnson P, et al; PHOENIX investigators. Randomized phase III trial of ibrutinib and rituximab plus cyclophosphamide, doxorubicin, vincristine, and prednisone in non-germinal center B-cell diffuse large B-cell lymphoma. *J Clin Oncol*. 2019;37(15):1285-1295.

37. Geiss GK, Bumgarner RE, Birditt B, et al. Direct multiplexed measurement of gene expression with color-coded probe pairs [published correction appears in *Nat Biotechnol* 2008;26:709]. *Nat Biotechnol*. 2008;26(3):317-325.

38. Scott DW, Wright GW, Williams PM, et al. Determining cell-of-origin subtypes of diffuse large B-cell lymphoma using gene expression in formalin-fixed paraffin-embedded tissue. *Blood*. 2014;123(8):1214-1217.

39. Masqué-Soler N, Szczepanowski M, Kohler CW, Spang R, Klapper W. Molecular classification of mature aggressive B-cell lymphoma using digital multiplexed gene expression on formalin-fixed paraffin-embedded biopsy specimens. *Blood*. 2013;122(11):1985-1986.

40. Szczepanowski M, Lange J, Kohler CW, et al. Cell-of-origin classification by gene expression and MYC-rearrangements in diffuse large B-cell lymphoma of children and adolescents. *Br J Haematol*. 2017;179(1):116-119.

41. Cascione L, Rinaldi A, Chiappella A, et al. Diffuse large B cell lymphoma cell of origin by digital expression profiling in the REAL07 Phase 1-2 study. *Br J Haematol*. 2018;182(3):453-456.

42. Klanova M, Sehn LH, Bence-Bruckler I, et al. Integration of cell of origin into the clinical CNS International Prognostic Index improves CNS relapse prediction in DLBCL. *Blood*. 2019;133(9):919-926.

43. Bolen CR, Klanova M, Trneny M, et al. Prognostic impact of somatic mutations in diffuse large B-cell lymphoma and relationship to cell-of-origin: data from the phase III GOYA study. *Haematologica*. 2019;haematol.2019.227892.

44. Nowakowski GS, Chiappella A, Witzig TE, et al. Variable global distribution of cell-of-origin from the ROBUST phase 3 study in diffuse large B-cell lymphoma. *Haematologica*. 2020;105(2):e72-e75.

45. King RL, Nowakowski GS, Witzig TE, et al. Rapid, real time pathology review for ECOG/ACRIN 1412: a novel and successful paradigm for future lymphoma clinical trials in the precision medicine era. *Blood Cancer J*. 2018;8(3):27.

46. Veldman-Jones MH, Lai Z, Wappett M, et al. Reproducible, quantitative, and flexible molecular subtyping of clinical DLBCL samples using the NanoString nCounter system. *Clin Cancer Res*. 2015;21(10):2367-2378.

47. Scott DW, Mottok A, Ennishi D, et al. Prognostic significance of diffuse large B-cell lymphoma cell of origin determined by digital gene expression in formalin-fixed paraffin-embedded tissue biopsies. *J Clin Oncol*. 2015;33(26):2848-2856.

48. Abdulla M, Hollander P, Pandzic T, et al. Cell-of-origin determined by both gene expression profiling and immunohistochemistry is the strongest predictor of survival in patients with diffuse large B-cell lymphoma. *Am J Hematol*. 2020;95(1):57-67.

49. Kendrick S, Tus K, Wright G, et al. Diffuse large B-cell lymphoma cell-of-origin classification using the Lymph2Cx assay in the context of BCL2 and MYC expression status. *Leuk Lymphoma*. 2016;57(3):717-720.

50. Phang KC, Akhter A, Tizen NMS, et al. Comparison of protein-based cell-of-origin classification to the Lymph2Cx RNA assay in a cohort of diffuse large B-cell lymphomas in Malaysia. *J Clin Pathol*. 2018;71(3):215-220.

51. Jais JP, Molina TJ, Ruminy P, et al. Reliable subtype classification of diffuse large B-cell lymphoma samples from GELA LNH2003 trials using the Lymph2Cx gene expression assay. *Haematologica*. 2017;102(10):e404-e406.

52. Staiger AM, Ziepert M, Horn H, et al; German High-Grade Lymphoma Study Group. Clinical impact of the cell-of-origin classification and the MYC/ BCL2 dual expresser status in diffuse large b-cell lymphoma treated within prospective clinical trials of the German High-Grade Non-Hodgkin's Lymphoma Study Group. *J Clin Oncol*. 2017;35(22):2515-2526.

53. Hwang HS, Yoon DH, Hong JY, et al. The cell-of-origin classification of diffuse large B cell lymphoma in a Korean population by the Lymph2Cx assay and its correlation with immunohistochemical algorithms. *Ann Hematol*. 2018;97(12):2363-2372.

54. Schouten JP, McElgunn CJ, Waaijer R, Zwijnenburg D, Diepvens F, Pals G. Relative quantification of 40 nucleic acid sequences by multiplex ligation-dependent probe amplification. *Nucleic Acids Res*. 2002;30(12):e57.

55. Mareschal S, Ruminy P, Bagacean C, et al. Accurate classification of germinal center B-cell-like/activated B-cell-like diffuse large B-cell lymphoma using a simple and rapid reverse transcriptase-multiplex ligation-dependent probe amplification assay: a CALYM study. *J Mol Diagn*. 2015;S1525-1578(15)00046-X.

56. Bobée V, Ruminy P, Marchand V, et al. Determination of molecular subtypes of diffuse large B-cell lymphoma using a reverse transcriptase multiplex ligation-dependent probe amplification classifier: a CALYM study. *J Mol Diagn*. 2017;19(6):892-904.

57. Lossos IS, Czerwinski DK, Alizadeh AA, et al. Prediction of survival in diffuse large-B-cell lymphoma based on the expression of six genes. *N Engl J Med*. 2004;350(18):1828-1837.

58. Shipp MA, Ross KN, Tamayo P, et al. Diffuse large B-cell lymphoma outcome prediction by gene-expression profiling and supervised machine learning. *Nat Med*. 2002;8(1):68-74.

59. Leonard JP, Kolibaba KS, Reeves JA, et al. Randomized phase II study of R-CHOP with or without bortezomib in previously untreated patients with non-germinal center B-cell-like diffuse large B-cell lymphoma. *J Clin Oncol*. 2017;35(31):3538-3546.

60. Davies A, Cummin TE, Barrans S, et al. Gene-expression profiling of bortezomib added to standard chemoimmunotherapy for diffuse large B-cell lymphoma (REMoDL-B): an open-label, randomised, phase 3 trial. *Lancet Oncol*. 2019;20(5):649-662.

61. Schmitz R, Wright GW, Huang DW, et al. Genetics and pathogenesis of diffuse large B-cell lymphoma. *N Engl J Med*. 2018;378(15):1396-1407.

62. Chapuy B, Stewart C, Dunford AJ, et al. Molecular subtypes of diffuse large B cell lymphoma are associated with distinct pathogenic mechanisms and outcomes [published correction appears in *Nat Med* 2018;24:1290-1292]. *Nat Med*. 2018;24(5):679-690.

63. Amin AD, Peters TL, Li L, et al. Diffuse large B-cell lymphoma: can genomics improve treatment options for a curable cancer? *Cold Spring Harb Mol Case Stud*. 2017;3(3):a001719.

64. Reddy A, Zhang J, Davis NS, et al. Genetic and functional drivers of diffuse large B cell lymphoma. *Cell*. 2017;171:481-494.

65. Dubois S, Tesson B, Mareschal S, et al; Lymphoma Study Association (LYSA) investigators. Refining diffuse large B-cell lymphoma subgroups using integrated analysis of molecular profiles. *EBioMedicine*. 2019;48:58-69.

66. Wright GW, Wilson WH, Staudt LM. Genetics of diffuse large B-cell lymphoma. *N Engl J Med*. 2018;379(5):493-494.

67. Arthur SE, Jiang A, Grande BM, et al. Genome-wide discovery of somatic regulatory variants in diffuse large B-cell lymphoma. *Nat Commun*. 2018;9(1):4001.

68. Wright GW, Huang DW, Phelan JD, et al. A probabilistic classification tool for genetic subtypes of diffuse large B cell lymphoma with therapeutic implications. *Cancer Cell*. 2020;37:551-568.

69. Xu-Monette ZY, Wu L, Visco C, et al. Mutational profile and prognostic significance of TP53 in diffuse large B-cell lymphoma patients treated with R-CHOP: report from an International DLBCL Rituximab-CHOP Consortium Program Study. *Blood*. 2012;120(19):3986-3996.

70. Xu-Monette ZY, Li L, Byrd JC, et al. Assessment of CD37 B-cell antigen and cell of origin significantly improves risk prediction in diffuse large B-cell lymphoma. *Blood*. 2016;128(26):3083-3100.

71. Xu-Monette ZY, Xiao M, Au Q, et al. Immune profiling and quantitative analysis decipher the clinical role of immune-checkpoint expression in the tumor immune microenvironment of DLBCL. *Cancer Immunol Res*. 2019;7(4):644-657.

72. Irizarry RA, Bolstad BM, Collin F, Cope LM, Hobbs B, Speed TP. Summaries of Affymetrix GeneChip probe level data. *Nucleic Acids Res*. 2003;31(4):e15.

73. Tusher VG, Tibshirani R, Chu G. Significance analysis of microarrays applied to the ionizing radiation response. *Proc Natl Acad Sci USA*. 2001;98(9):5116-5121.

74. Eisen MB, Spellman PT, Brown PO, Botstein D. Cluster analysis and display of genome-wide expression patterns. *Proc Natl Acad Sci USA*. 1998;95(25):14863-14868.

75. Eraslan G, Avsec Ž, Gagneur J, Theis FJ. Deep learning: new computational modelling techniques for genomics. *Nat Rev Genet*. 2019;20(7):389-403.

76. Ching T, Himmelstein DS, Beaulieu-Jones BK, et al. Opportunities and obstacles for deep learning in biology and medicine. *J R Soc Interface*. 2018;15(141):15.

77. Sha C, Barrans S, Cucco F, et al. Molecular high-grade B-cell lymphoma: defining a poor-risk group that requires different approaches to therapy. *J Clin Oncol*. 2019;37(3):202-212.

78. Ennishi D, Jiang A, Boyle M, et al. Double-hit gene expression signature defines a distinct subgroup of germinal center B-cell-like diffuse large B-cell lymphoma. *J Clin Oncol*. 2019;37(3):190-201.

79. Bojarczuk K, Wienand K, Ryan JA, et al. Targeted inhibition of PI3Kα/δ is synergistic with BCL-2 blockade in genetically defined subtypes of DLBCL. *Blood*. 2019;133(1):70-80.

80. Oberg JA, Glade Bender JL, Sulis ML, et al. Implementation of next generation sequencing into pediatric hematology-oncology practice: moving beyond actionable alterations. *Genome Med*. 2016;8(1):133.

81. Du-Harpur X, Watt FM, Luscombe NM, Lynch MD. What is AI? Applications of artificial intelligence to dermatology. *Br J Dermatol*. 2020;bjd.18880.

82. Narrandes S, Xu W. Gene expression detection assay for cancer clinical use. *J Cancer*. 2018;9(13):2249-2265.

83. Zhang W, Yu Y, Hertwig F, et al. Comparison of RNA-seq and microarray-based models for clinical endpoint prediction. *Genome Biol*. 2015;16(1):133.